

Approaching the microjoule frontier with femtosecond laser oscillators: theory and comparison with experiment

V L Kalashnikov^{1,2,5}, E Podivilov³, A Chernykh³, S Naumov²,
A Fernandez², R Graf² and A Apolonski^{3,4}

¹ Institut für Photonik, TU Wien, Gusshausstr. 27/387, A-1040 Vienna, Austria

² Max-Planck-Institut für Quantenoptik, Hans-Kopfermann-Str. 1,
D-85748 Garching, Germany

³ Institute of Automation and Electrometry, RAS, 630090 Novosibirsk, Russia

⁴ Department für Physik der Ludwig-Maximilians-Universität München,
am Coulombwall 1, D-85748 Garching, Germany

E-mail: kalashnikov@tuwien.ac.at

New Journal of Physics **7** (2005) 217

Received 31 May 2005

Published 10 October 2005

Online at <http://www.njp.org/>

doi:10.1088/1367-2630/7/1/217

Abstract. A detailed numerical analysis of heavily chirped pulses in the positive-dispersion regime (PDR) is presented on the basis of the distributed cubic–quintic generalized complex nonlinear Ginzburg–Landau equation. It is demonstrated that there are three main types of pulse spectra: truncated parabolic-top, Π - and M-shaped profiles. The strong chirp broadens the pulse spectrum up to 100 nm for a Ti : Sa oscillator, which provides compressibility of the picosecond pulse down to sub-30 fs. Since the picosecond pulse has a peak power lower than the self-focusing power inside a Ti : Sa crystal, the microjoule energies become directly available from a femtosecond oscillator. The influence of the third- and fourth-order dispersions on the pulse spectrum and stability is analysed. It is demonstrated that the dynamic gain saturation plays an important role in pulse stabilization. The common action of dynamic gain saturation, self-amplified modulation (SAM) and saturation of the SAM provides pulse stabilization inside the limited range of the positive group-delay dispersions (GDDs). Since the stabilizing action of the SAM cannot be essentially enhanced for a pure Kerr-lens mode-locking regime, a semiconductor saturable absorber is required for

⁵ Author to whom any correspondence should be addressed.

pulse energies of $>0.7 \mu\text{J}$ inside an oscillator. The basic results of the numerical analysis are in an excellent agreement with experimental data obtained from oscillators with repetition rates ranging from 50 to 2 MHz.

Contents

1. Introduction	2
2. Model	3
3. Results of modelling	5
3.1. High-energy solitary pulse in the PDR	6
3.2. Variation of the pulse parameters with GDD	6
3.3. Pulse chirp and its compensation	6
3.4. Spectrum profile	9
4. Comparison with experimental results and discussion	10
4.1. Spectral shape	10
4.2. Chirp.	11
4.3. Gain saturation and pulse stability	12
4.4. Energy limits	13
4.5. PDR for oscillators with common pulse repetition rate	14
4.6. Self-similar pulses and the PDR.	14
5. Conclusion	14
Acknowledgments	15
References	15

1. Introduction

It was experimentally demonstrated in a previous paper [1] that a Kerr-lens mode-locked Ti : Sa oscillator operating in the positive-dispersion regime (PDR) may provide a feasible route for producing microjoule femtosecond pulses at MHz repetition rates. This regime is a challenge to theoretical analysis because its description requires careful study of both the linear and nonlinear factors affecting the heavily chirped pulse dynamics. It has been proposed that high-energy pulses in the PDR can be provided by self-similarity phenomena, i.e. by self-reproducible oscillation of a subpicosecond or picosecond pulse in the presence of group-delay dispersion (GDD) and self-phase modulation (SPM) varying along a propagation axis [2, 3]. This regime tolerates strong nonlinearities causing a variety of instabilities that limit further pulse power growth. Nevertheless, as will be demonstrated in this paper, the high-energy generation in the PDR can be explained by formation of the heavily chirped pulse, which behaves like a soliton and does not need variation of the dispersion within the oscillator in order to provide its stability.

In this paper, we present a systematical theoretical study of the PDR in a Ti : Sa oscillator. Our theoretical analysis based on the distributed complex cubic–quintic Ginzburg–Landau equation reveals the basic properties of the regime considered: a variety of different stable spectra (parabolic-like, flat-top and M-shaped spectral profiles), strong chirp greatly increasing at the spectrum edges, decisive contribution of the dynamic gain saturation to pulse stability.

Comparison with the experiment allows careful estimation of the model parameters and determination of the energy limits inherent in the PDR. The influence of GDD (up to fourth order) and of saturation of self-amplitude modulation (SAM) on the pulse spectrum and its stability was demonstrated. It was found that a saturable Bragg reflector (SBR) is required for stabilization of the oscillator with sub-10 MHz pulse repetition rates.

2. Model

Usually, an adequate description of pulse generation in the negative net-GDD region is based on a quasi-soliton model (see e.g. [4]–[6]) taking into account spectral filtering, GDD distributed along the oscillator cavity, saturable gain, linear loss, SPM and SAM due to Kerr lensing inside an active medium. The last factor can usually be described only approximately because it depends on the cavity geometry, pump conditions etc [7, 8]. Hence a precise description of the spatio-temporal femtosecond dynamics requires full-dimensional simulations [9, 10]. Nevertheless, the main characteristics of Kerr-lens mode-locked lasers such as pulse duration and energy, spectrum, stability etc. can be obtained on the basis of a one-dimensional (1D) model treating the mode-locking effect of the Kerr lensing as the cubic amplitude nonlinearity distributed over the cavity [5, 11]. Modelling of high-energy oscillators needs to take into account higher order nonlinear terms for SAM (for example, the quintic amplitude term or some other modifications; see [5, 12, 13]). In the framework of a 1D quasi-soliton model, a non-uniform distribution of the intracavity nonlinearity and dispersion can be successfully modelled [14]. There are no basic obstacles to explore 1D distributed models in the PDR [4], although some generalizations of the master equation may be required [3], [15]–[17].

Our numerical analysis is based on the generalized cubic–quintic complex Ginzburg–Landau equation (basic abbreviations, symbols and simulation parameters are presented in tables 1 and 2):

$$\begin{aligned} \frac{\partial a(z, t)}{\partial z} = & -\sigma(E)a(z, t) + (\tau_s(E) + i\beta_2)\frac{\partial^2 a(z, t)}{\partial t^2} + \beta_3\frac{\partial^3 a(z, t)}{\partial t^3} \\ & - i\beta_4\frac{\partial^4 a(z, t)}{\partial t^4} + (\kappa - i\gamma)|a(z, t)|^2 a(z, t) - \kappa\zeta|a(z, t)|^4 a(z, t). \end{aligned} \quad (1)$$

Here, z is the longitudinal coordinate (i.e. the round-trip number after normalization to the cavity length L_{cav}), t is the local time measured from the pulse centre at $t = 0$, and $|a|^2 = P$ is the pulse power. Parameter $\sigma(E) = \delta - \alpha/\sqrt{1 + 2E/E_s}$ is the difference of the round-trip amplitude loss δ and the gain α saturated by the full energy of the pulse $E(z) = \int_{-T_{\text{cav}/2}}^{T_{\text{cav}/2}} |a(z, t')|^2 dt'$ (T_{cav} is the cavity period), and $E_s = I_s T_{\text{cav}} S$ is the gain saturation energy (I_s is the gain saturation intensity, S is the effective beam waist area inside the crystal). Parameter σ plays an important role in pulse stability against cw generation and will therefore be referred to henceforth as the stability parameter.

Saturable gain is the decisive factor in pulse stabilization (see section 4.3). The dependence of the saturable gain on the energy in equation (1) is affected by the mode variation inside the active crystal since the intensity along the propagation axis is inversely proportional to the mode area depending on z . Then for a Gaussian mode the saturable gain has the form of equation (1) (i.e. $\propto 1/\sqrt{1 + 2E/E_s}$) in the limit where the confocal length is much less than the crystal length. This situation corresponds to the experiment and only such a form of the saturable gain

Table 1. Basic abbreviations and symbols.

PDR	Positive-dispersion regime
GDD	Group-delay dispersion
SBR	Saturable Bragg reflector
SPM	Self-phase modulation
SAM	Self-amplitude modulation
β_i	Taylor expansion coefficients in GDD approximation, $i = 2, 3, 4$
β_2^*	Dispersion providing the transitional Π -like spectrum
σ	Stability parameter
σ_{th}	Threshold stability parameter
ω	Shift from the carrier frequency; 0.1 fs^{-1} corresponds to 33 nm
α	Gain coefficient
τ_s	Saturable gain bandwidth parameter, fs^2
κ	SAM parameter (cubic SAM)
ζ	Parameter of SAM saturation (quintic SAM)
T	Pulse duration, fs
Δ	Pulse spectrum bandwidth; dimension as ω
E	Pulse energy
E_s	Gain saturation energy
Q	Chirp at the pulse peak, fs^2
ψ	Dimensionless chirp, $\psi \simeq T\Delta/4 \simeq Q\Delta^2/2$
Q_{fd}	Frequency-dependent chirp ($Q_{\text{fd}} \equiv (1/2)d^2\phi(\omega)/d\omega^2$, $\phi(\omega)$ is the spectral phase)
P_{av}	Average power
P_{peak}	Peak power
P_{p}	Pump power
T_{cav}	Cavity period

Table 2. Parameters of the 10 MHz Ti : Sa oscillator (pump power $P_{\text{p}} = 10 \text{ W}$, 0.28 output loss).

τ (fs^2)	γ (MW^{-1})	P_{sf} (MW)	δ	α	λ (μm)	I_s (MW cm^{-2})	S (μm^2)	T_{cav} (ns)	β_4 (fs^4)
5	4.55	1.3	0.22	0.95	0.79	0.25	260	100	2000

provides results which agree with the experimental data. An inverse relation between the crystal and confocal lengths gives the gain term [5].

The saturable gain bandwidth parameter has the form $\tau_s(E) = \tau\alpha/\sqrt{1+2E/E_s}$, where parameter τ describes the spectral gain profile and is defined by twofold decrease of the gain due to spectral deviation from the maximum of the gain profile. For example, the value of $\tau = 5 \text{ fs}^2$ corresponds to 300 nm gain bandwidth. Parameters β_2 , β_3 and β_4 approximate the net cavity dispersion, which depends on the frequency: $L_{\text{cav}}(d^2k/d\omega^2) = \beta_2 + 3\beta_3\omega + 6\beta_4\omega^2$ (k is the wave number, ω is the angular frequency shift measured from the maximum of the gain profile). The SPM of the time-dependent field with instant power $P(t)$ inside the crystal is defined as $(2\pi n_0 n_2/\lambda_0)P(t) \int \frac{dz}{S(z)} = \gamma P(t)$, where we integrate over the active crystal length. For a Gaussian beam, in the considered limit of a short confocal parameter we have $\gamma = 4\pi^2 n_0 n_2/\lambda_0^2$. Here, $n_0 = 1.75$ is the linear refractive index of Ti : Sa, λ_0 is the wavelength corresponding to the

gain maximum, and $n_2 = (5.2 \pm 1) \times 10^{-16} \text{ W cm}^{-2}$ [18] is the nonlinear refraction index. The best agreement with the experimental values of the chirp and the spectrum widths is provided by the value of $n_2 = 4.2 \times 10^{-16} \text{ W cm}^{-2}$. Parameters κ and ζ define the cubic and the quintic SAM terms, respectively.

The main challenge is to estimate the SAM parameters κ and ζ . These parameters cannot be directly measured, but an indirect estimate of κ can be obtained from the measured values of the pulse chirp $Q \simeq 8000 \text{ fs}^2$ and its spectral width $\Delta \simeq 0.15 \text{ fs}^{-1}$ [1]. The soliton-like solution of the cubic version of equation (1) with $\beta_3 = 0$, $\beta_4 = 0$ and $\zeta = 0$ obeys [19]: $\kappa/\gamma \simeq 3/Q\Delta^2 \approx 0.02$. This value is lower than that indirectly measured for a hard-aperture Kerr-lens mode-locked Ti : Sa oscillator [20] and close to the values calculated for soft-aperture mode-locked lasers [7]. Parameter κ can be varied by changing both the cavity geometry and the beam size inside the crystal and it strongly influences the transition from Π -like to M-like spectra due to variation of β_2 (see section 4.1). A comparison of this transition with the experimental value of β_2 gives $\kappa/\gamma \approx 0.04$.

The quintic term in equation (1) was introduced in order to provide saturable SAM. Saturable SAM has been widely applied for analysis of additive-pulse mode-locking [5, 21, 22]. It is clear that self-focusing in the Kerr-lens mode-locking regime improves the overlap of the pump and the oscillator beams only up to some limit where the oscillator beam size becomes smaller than the pump one. Since both κ and ζ result from a common effect of self-focusing, ζ is related to κ and cannot be varied quite independently (see [13] in contrast to the approach [23], for example). In fact, the maximum peak pulse power P_{max} has an upper limit equal to $1/\zeta$ and has to be lower than the threshold power of self-focusing $P_{\text{sf}} \approx 1.9\lambda_0^2/(4\pi n_0 n_2) = 1.3 \text{ MW}$. The best agreement with the experimental pulse duration is provided by the value of $\zeta \approx 3.6/P_{\text{sf}}$, i.e. $\zeta = 0.6\gamma$, which agrees with the qualitative estimation $\zeta \simeq 1/P_{\text{max}} \approx T/E$ ($T \simeq 2 \text{ ps}$ is the intracavity pulse duration and $E \simeq 660 \text{ nJ}$ for the 10 MHz oscillator [24]). Direct calculations based on the generalized nonlinear ABCD method [7] suggest that SAM can be saturated by the peak power ranging between 0.2–0.8 MW, which is close to our estimation.

We searched the static pulse-like solutions of equation (1) for different values of κ/γ , ζ , β_3 and β_4 and compared the dependencies of the pulse energy and duration, the spectrum shape and width, and the chirp on β_2 with the experimental ones. This allowed the unknown parameters of SAM to be defined. The numerical method was based on the split-step Fourier method, the time window being 330 ps. As an initial condition, a superposition of cw solutions corresponding to $\sigma(E) = 0$ and eight Gaussian pulses with random small amplitudes and positions was used. Usually, 5000 iterations corresponding to 0.5 ms of the build-up evolution were sufficient to provide a static solution. After formation of the pulse, its parameters were chosen as an initial condition for the adiabatic variation of the parameters of equation (1).

3. Results of modelling

The results of numerical simulations based on the above-described model are summarized in this section. It is shown that large chirp of a pulse causes both spectral and temporal pulse broadening. The former provides femtosecond durations after pulse compression; the latter reduces the peak power and thereby stabilizes the pulse. We analyse the generation of a high-energy static pulse in the PDR for the example of an oscillator with 10 MHz pulse-repetition rate [24].

3.1. High-energy solitary pulse in the PDR

As is well known, the existence of a solitary (static) pulse in the PDR was predicted by Haus *et al* [4]. Such a pulse is the soliton-like solution of the cubic complex Ginzburg–Landau equation and can be stabilized against cw generation. However, our simulations demonstrated that the main source of high-energy (>200 nJ) pulse destabilization is the explosive instability, where the pulse intensity rapidly increases and, as a result, the pulse collapses. The cause of such behaviour is the absence of SAM saturation. For low-energy pulses (10–20 nJ) the stability can be provided by gain saturation, spectral filtering or GDD. However, high-energy pulses have a peak power which approaches P_{sf} . Hence self-focusing essentially changes the oscillator mode so that the cubic version of equation (1) loses its validity. Reduction of overlapping between the pump and the oscillator modes caused by the strong self-focusing can be considered as SAM saturation and described by the cubic–quintic version of equation (1). We found that only such a generalization of the model can explain the stable pulses observed in the PDR.

3.2. Variation of the pulse parameters with GDD

Our simulations demonstrated that variation of the GDD distribution [25] within the oscillator under consideration causes very weak pulse breathing (within just a few per cent). The crystal dispersion compensation in the symmetric (negative dispersion is symmetrically distributed on both sides of the crystal) or the asymmetric (all negative dispersion is located on one side of the crystal) configurations results in pulse parameters which are precisely reproducible in the framework of the distributed model. This work is therefore based only on this model (see equation (1)).

Let us consider variation of the main pulse parameters with the dispersion. Figure 1(a) shows the pulse chirp (at $t = 0$, i.e. at the pulse peak). The chirp increases monotonically and rapidly with the dispersion. Obviously, the appearance of strong chirp results from the cumulative phase action of SPM and dispersion [15] in contrast to the reciprocal phase compensation in the negative-dispersion regime. The chirp and pulse durations increase with β_2 , whereas the spectrum becomes narrower (figure 1(b), black and red curves, respectively).

In accordance with the experiment, dependence of the pulse energy on β_2 is comparatively weak: the pulse energy increases with dispersion and alters within 5% in the considered range of variation of β_2 . The upper intracavity energy limit is $P_{\text{av}}T_{\text{cav}}/0.28 = 660$ nJ for 1.8 W output average power P_{av} , where 0.28 is the output loss.

3.3. Pulse chirp and its compensation

Our calculations demonstrate that a simple relation for the dimensional chirp $Q \simeq T/2\Delta$, which resembles that for the sech-pulse solution of the cubic version of equation (1), is approximately valid. The validity of such a simple relation means that the contribution of the frequency-dependent chirp Q_{fd} (table 1) is comparatively small (see below).

Nevertheless, Q_{fd} rapidly increases at the pulse spectrum edges (figure 2(a) presents the spectral dependence of the chirp normalized to its minimum value). Such a nonlinear dependence is intensified as $\beta_2 \rightarrow 0$. In figure 2(a), the black curve corresponds to $\beta_2 = 110$ fs² and can be characterized as a higher order parabolic-like dependence on the frequency providing a slight rise of the chirp in the vicinity of the central frequency. The red curve corresponds to $\beta_2 = 70$ fs² and has a lower order parabolic-like dependence giving a comparatively fast rise of the chirp near the central frequency.

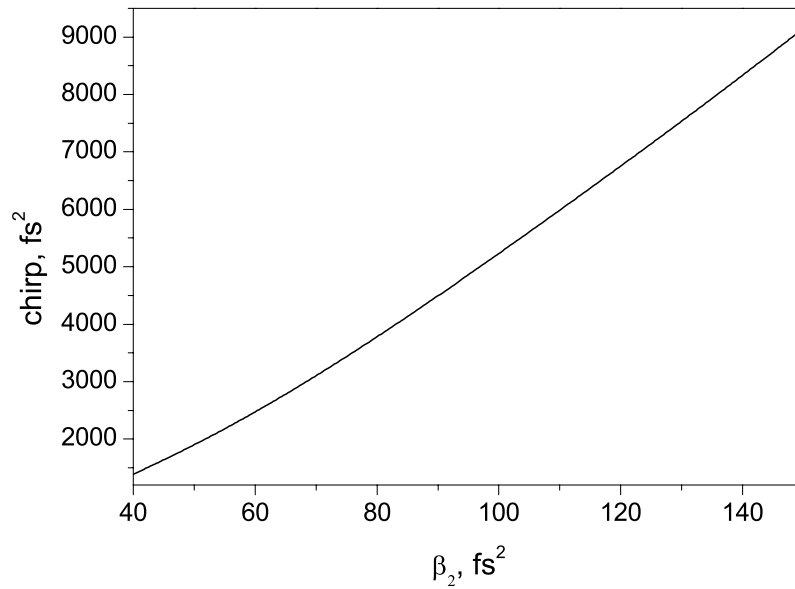
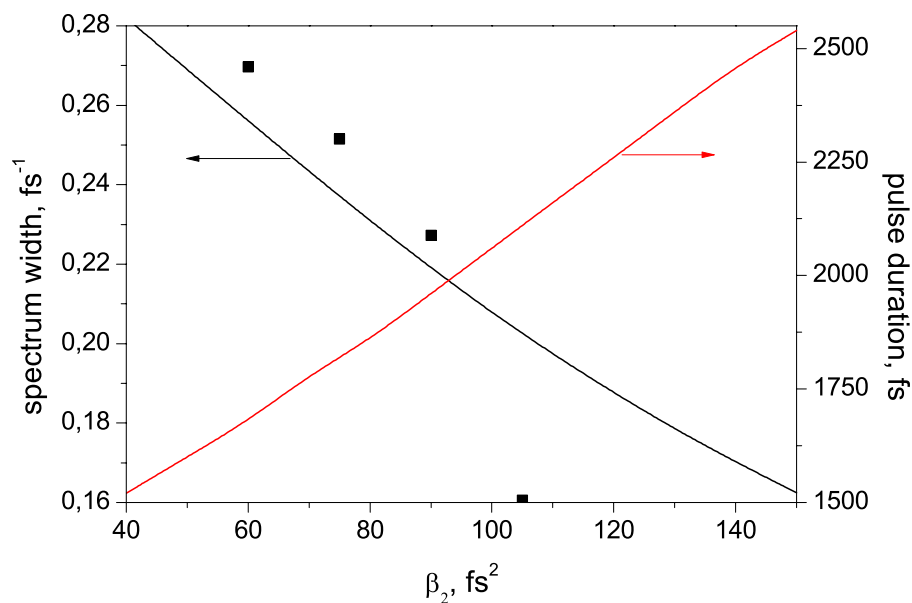
a*b*

Figure 1. Calculated dependencies of pulse chirp (a), spectral width (b, black curve) and duration (b, red curve) on dispersion for the oscillator with 10 MHz pulse repetition rate. Points correspond to the experimental spectral widths.

Almost constant and minimal chirp in the vicinity of λ_0 can be perfectly compensated. This gives a femtosecond chirp-free pulse containing most of the energy (red curve in figure 2(b)). The black curve in figure 2(b) shows the pulse profile before compression; the black curve in

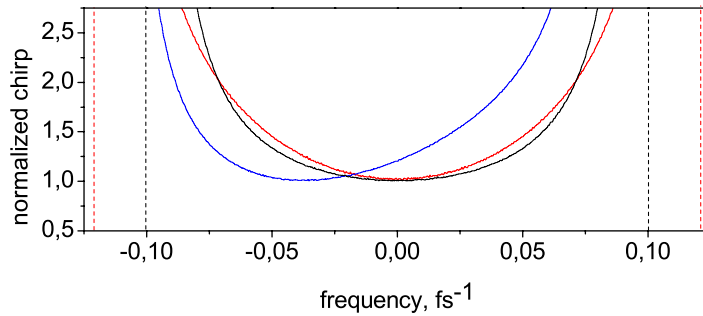
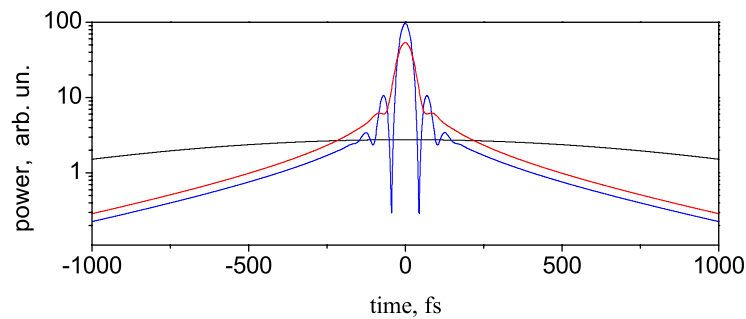
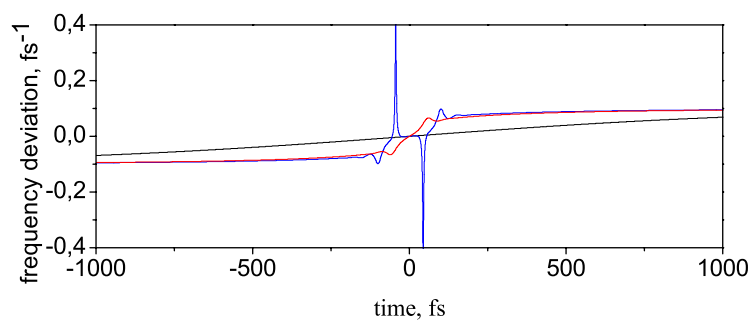
a*b**c*

Figure 2. Frequency-dependent chirp (a), pulse profiles after compression (b) and frequency deviation (c). (a): $\beta_2 = 110 \text{ fs}^2$ (black), 70 fs^2 (red), $\beta_3 = 0$ (black, red), 300 fs^3 (blue). (b): $\beta_2 = 110 \text{ fs}^2$, pulse power profile before compression (black), after compression with -6000 fs^2 (red) and -6600 fs^2 (blue) compensating dispersion. (c): frequency deviation before compression (black), after compression with -6000 fs^2 (red) and -6600 fs^2 (blue) compensating dispersion; $\beta_2 = 110 \text{ fs}^2$. Dashed lines in (a) show edges of the corresponding spectra.

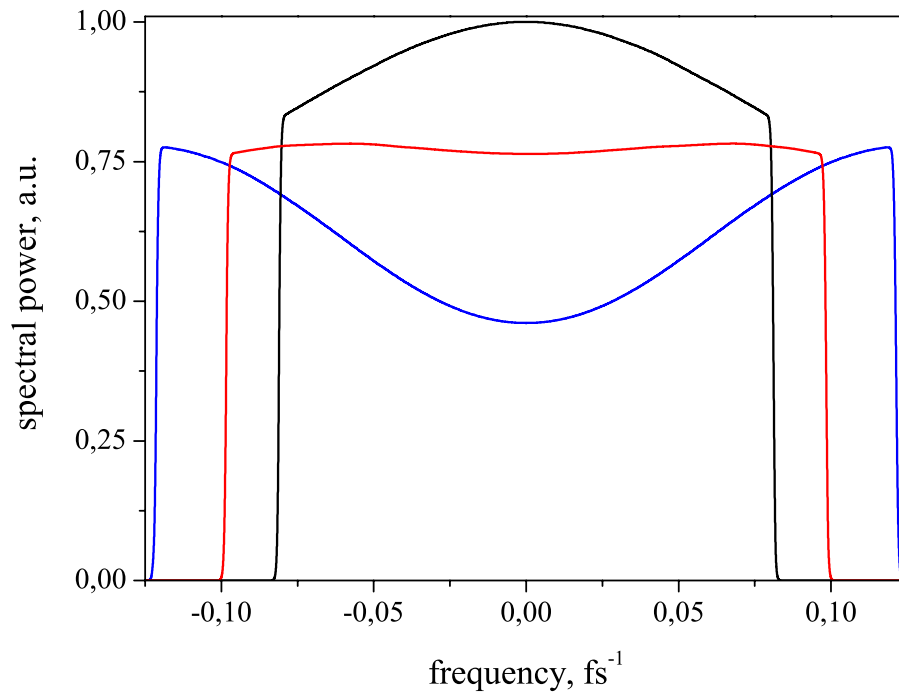


Figure 3. Calculated spectral profiles for $\beta_2 = 150 \text{ fs}^2$ (black), 110 fs^2 (red), 70 fs^2 (blue), $\beta_3 = 0 \text{ fs}^3$ and $\beta_4 = 2000 \text{ fs}^4$.

figure 2(c) shows the corresponding time-dependence of the frequency deviation. Non-constant chirp at the spectrum wings leads to the appearance of bell-like wings with uncompensated chirp and large frequency deviation (red one at the pulse front and blue one at its tail, red curve in figure 2(c)). The peak power increases with the dispersion of the compressor, but at the price of satellites appearing (blue curve in figure 2(b)). These satellites contain the spectral components which strongly deviate from the central frequency (blue curve in figure 2(c)). Further increase of the compensating dispersion causes pulse fragmentation.

3.4. Spectrum profile

Let us now consider the effect of GDD on the spectrum profile (figure 3). With decreasing β_2 , the spectrum profile changes from parabolic-top (black curve) to Π -shaped (red curve) and then to M-shaped (blue curve). Since the pulse spectrum is quite broad in PDR, it is strongly affected by high-order dispersion. Thus, the M-shaped spectrum for near-zero β_2 is formed by enhancement of the spectral components at the spectrum edges due to the contribution of positive fourth-order dispersion. The fourth-order dispersion β_4 enhances M-shaping and decreases the spectrum width (black curve in figure 4; for comparison, the red curve shows the spectrum in the absence of high-order dispersion). Third-order dispersion shifts the centre of gravity of the spectrum towards the dispersion minimum, whereas the maximum of the spectrum tends to the dispersion maximum (blue curve in figure 4; compare with figure 4(b) in [1]). The point of the chirp minimum is located in the vicinity of the dispersion minimum (blue curve in figure 2). The contribution of high-order dispersions enhances chirp variation with frequency.

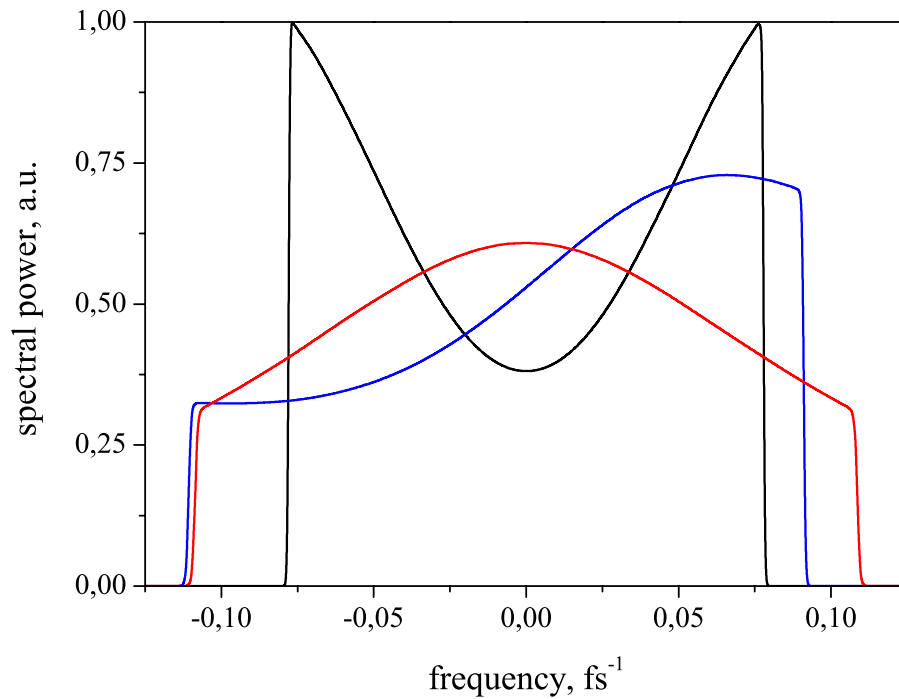


Figure 4. Calculated spectral profiles for $\beta_2 = 110 \text{ fs}^2$, $\beta_4 = 0 \text{ fs}^4$ (red), 2000 (blue), 10000 (black), $\beta_3 = 0 \text{ fs}^3$ (black, red), 300 (blue).

We also found a non-trivial effect of fourth-order dispersion on pulse stability: moderate positive β_4 (which corresponds to the local minimum of dispersion under the gain maximum) enhances stability for small β_2 , whereas even small negative β_4 destabilizes the pulse at any positive β_2 .

4. Comparison with experimental results and discussion

4.1. Spectral shape

The considered cubic–quintic complex Ginzburg–Landau model with saturable gain describes all essential characteristics of the chirped-pulse regime. First of all, the decrease of positive GDD transforms the spectral shapes from parabolic-like to Π -like and then to M-like ones. This transformation is clearly visible both in the calculations (figure 3) and in the experiment (figure 5(b) in [1]). The parameter that determines the dispersion β_2^* , which by definition is the dispersion providing the ‘transitional’ Π -like spectrum, is the relative cubic nonlinearity κ/γ . The growth of κ shifts β_2^* towards zero. We obtained an estimate for $\kappa/\gamma \simeq 0.04$ by comparison with the experimental value of β_2^* .

Qualitatively such influence of κ on the spectral shape can be described in the following way: growth of κ for a given GDD increases the Kerr-lens-induced efficient gain (which is proportional to κP) at the pulse peak, where the central spectral components are located in the chirped pulse. This enhances the central part of the spectrum and creates its parabolic-like shape.

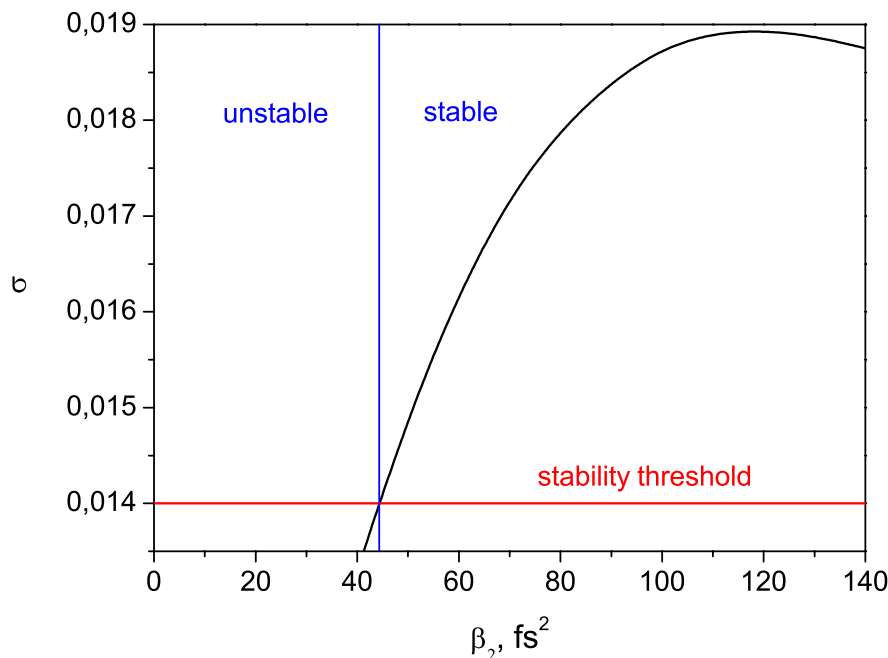


Figure 5. Dependence of the stability parameter σ on dispersion. The stability threshold (σ_{th}) is determined by the dynamic gain saturation (see text).

The M-shaped spectra can be attributed to the fourth-order dispersion action which prevails in the vicinity of zero β_2 . Experimentally observable asymmetry of the spectra (figure 4(b) in [1]) is produced by third-order dispersion.

One has to note that the negative dispersion regime in the vicinity of zero GDD can reproduce some spectral properties of the PDR. A shift of negative GDD to zero in the presence of positive fourth-order dispersion pushes the zero-dispersion points towards the pulse spectrum. This in turn moves the dispersion–wave spectral spikes to the main spectrum and intensifies them. As a result, some analogue of M-like spectra appears. However, the autocorrelation demonstrates that this regime is unstable, i.e. the pulse suffers strong transformation during propagation.

Comparison of the calculated spectral widths (black line in figure 1(b)) with the experimental ones (points in figure 1(b)) shows good agreement with the exception of the stability border for large β_2 (see section 4.3).

4.2. Chirp

Insight into the chirp behaviour can be provided by the cubic version of equation (1) in the absence of high-order dispersion. In the limit of $\psi \gg 1$ the sech-like solution $\propto [\cosh(2t/T)]^{i\psi-1}$ of the cubic Ginzburg–Landau equation possesses

$$\psi = \frac{3}{\frac{\tau_s}{\beta_2} + \frac{\kappa}{\gamma}}, \quad (2)$$

which gives the growth of the dimensionless chirp ψ with the dispersion and inversely proportional to κ/γ . Simultaneously, the γ value affects the spectrum width. Since the parameter

κ/γ can be obtained from the experimental value of β_2^* (see above), a comparison with the experimental values of both the chirp Q and spectral widths suggests the γ value, which corresponds to the lower limit of n_2 reported in [18].

Dependence of the chirp on the frequency is an important property of PDR. Such frequency-dependent chirp Q_{fd} grows rapidly with the frequency in the vicinity of the spectrum edges. Variation of β_2 allows control of the width of the region inside the pulse spectrum, where the chirp is almost frequency-independent. The wider spectrum obtained in the vicinity of zero dispersion possesses a stronger dependence of the chirp on the frequency. High-order dispersions enhance Q_{fd} . The presence of Q_{fd} makes pulse compression more difficult and causes the appearance of satellites which are spectrally shifted from the central frequency.

Saturation of SAM in the model plays the role of a pulse power limiter: the maximum peak power is less than $1/\zeta$. Hence the quintic term determines the relation between the pulse energy and its duration. In the experiment, the maximum intracavity peak power is ≈ 0.3 MW, which explains our choice of ζ . This value gives the best agreement with the experimentally observed pulse energy and duration.

4.3. Gain saturation and pulse stability

It should be noted once more that the experimentally observed pulse energies can be numerically reproduced only if we introduce the square-root dependence in the term describing the gain saturation (saturable gain $\propto 1/\sqrt{1+2E/E_s}$; see equation (1)). Such dependence is determined by strong focusing inside the active crystal so that the beam confocal length is much less than the crystal length.

The most important characteristic of the PDR is its stability against multipulsing and cw generation. In low-energy oscillators with high-pulse repetition rate, gain saturation accumulates in the process of multiple passing of the pulse through an active medium. Single-pass saturation (i.e. dynamic gain saturation) is small and the stability criterion against cw generation is $\sigma > 0$. This means that there is net loss only outside the pulse. In the negative dispersion range for the cubic version of equation (1), this results in the requirement $|\psi| < 1$. In contrast, the corresponding stability criterion in the PDR leads to $\psi \gg 1$, which gives the duration–bandwidth product $T\Delta \gg 1$.

In our case, the dynamic gain saturation is a noticeable effect and the saturation parameter has to compensate the gain difference between the pulse front and its tail. The constraint on σ is stricter for high-energy oscillators: $\sigma > \sigma_{th} \simeq \alpha T_{cav}/(2T_r)$ (e.g. $\sigma_{th} \approx 0.014$ for the considered example, $T_r \approx 3.5 \mu s$ is the gain relaxation time). The dependence of σ on β_2 is shown in figure 5. Since the dynamic gain saturation is proportional to α , the threshold stability parameter σ_{th} increases with the pump power P_p . Hence, the minimal β_2 providing pulse stabilization increases with P_p in agreement with experimental observation [1].

On the one hand, pulse stability breaks in the vicinity of zero β_2 . This destabilization is caused by suppressed gain saturation due to the pulse energy decrease (within only a few per cent; see section 3.1) with $\beta_2 \rightarrow 0$. Such a reduction of the energy results from growing spectral loss since $\beta_2 \rightarrow 0$ leads to spectrum broadening (see black line in figure 1(b)). So, destabilization imposes a limit on the achievable spectrum width.

On the other hand, the pulse power reduction, caused by the longer pulse at larger β_2 , decreases the efficiency of SAM formed by self-focusing in the crystal. As a result, the pulse energy decreases as the dispersion value increases, which reduces the gain saturation. There is

some β_2 that provides the maximum pulse stability (this is 120 fs² in our example; see figure 5) and larger dispersion values destabilize the pulse. In the experiment, such destabilization occurs immediately after the stability maximum, which cannot be described in the framework of our model and needs to take into account the time-dependence of σ due to the dynamic gain saturation. Exactly these effects impose a limit on the longest pulses achievable.

It was found numerically that the stability parameter σ increases almost linearly with κ/γ . This gives an additional estimate of the SAM parameter. Thus $\kappa/\gamma < 0.02$ gives the maximum $\sigma < 0.014$, i.e. the PDR is unstable (figure 5). For $\kappa/\gamma = 0.06$ the stability range shifts to zero GDD so that the spectrum with 110 nm width is stable. However, such a wide spectrum was not attainable in the experiment. Hence, the parameter κ/γ ranges between 0.02 and 0.06.

Since the gain is maximal before the pulse front, the rise of perturbations begins in front of the pulse. This creates a cw-like pedestal (figure 3 in [1]) which expands with P_p , absorbs the pump energy and forms a narrow-band spectral spike in the vicinity of λ_0 . If SAM is sufficiently strong, the cw perturbation can entail a new picosecond pulse that, after some transient process, results in doubling of the pulse-repetition frequency.

4.4. Energy limits

The maximum pulse energy is limited from above by the average power P_{av} : $E_{max} \simeq P_{av} T_{cav}$. At the same time, the pulse peak power $P_{peak} \simeq P_{av} T_{cav}/T$ has to be $< P_{sf}$ (we operate close to this threshold in the oscillator generating 500 nJ pulses). Practically, the output average power (1.8 W in the 10 MHz oscillator) cannot be essentially increased due to the pump power growth, but one way to achieve higher energy would be to reduce the pulse-repetition rate. However, we have to obey the relation $P_{peak} < P_{sf}$, which can only be achieved with long pulses.

Since the active crystal is thin (3 mm in our case), the beam does not collapse even at the peak power $\approx P_{sf}$. However, we can suppose that this does not allow the peak power to be essentially increased. In fact, strong focusing of the pump produces a diffraction-divergent beam within the crystal but, simultaneously, the laser beam is convergent due to the self-focusing. As a result, the beams overlapping becomes worse for $P_{peak} > P_{sf}$, which prevents further peak-power growth.

In the negative dispersion regime long pulses can be obtained due to the large value of $|\beta_2|$ [26]. However, this reduces the spectrum width since the pulse chirp is necessarily zero. Of course, such a frequency-limited pulse does not permit further compression. In the PDR the chirp is not zero (in our experiments $\psi = T\Delta/4 \simeq 2 \text{ ps} \times 0.2 \text{ fs}^{-1}/4 = 100$). This allows a wide spectrum even for a long pulse. As a result of large chirp, sub-40 fs pulses can be obtained after compression (a compressed pulse has the duration $\simeq 1/\Delta$). For equal durations of the soliton-like pulse (negative dispersion region) and the compressed chirped pulse (PDR), we have a 100-fold gain in energy for the latter in comparison with the former due to the essentially longer pulse and, consequently, reduced peak power of the chirped pulse before compression ($T = 4\psi/\Delta$).

However, in practice long high-energy pulses face a challenge to pulse stability at a large value of positive dispersion. The main effects which would provide pulse stabilization are SAM (κ , cubic term in equation (1)) and saturation of SAM (ζ , quintic term in equation (1)). The former increases the stability parameter σ and the latter confines the pulse peak power. Unfortunately, the parameters κ and ζ cannot be noticeably changed in a pure Kerr-lens mode-locking regime and therefore require SBR, which operates almost as a ‘fast’ saturable absorber for the picosecond pulses in the PDR (however, an analysis of SBR action would exceed the framework of our

model). The experiments [1] demonstrate that this is a correct strategy to stabilize the high-energy pulses in low-repetition rate oscillators.

4.5. PDR for oscillators with common pulse repetition rate

Although the chirped-pulse regime provides high-energy pulses directly from a low-repetition rate oscillator, its basic characteristics are not governed by the oscillator repetition rate. This regime can also be realized in conventional short-cavity oscillators. Realization of this regime can be seen from figure 2 in [1]. The pulse characteristics are $T \approx 1.5$ ps, $\Delta \approx 0.1$ fs⁻¹ and $E = 50$ nJ for 50 MHz repetition rate. As was pointed out, the basic characteristic of the PDR is $\psi \gg 1$. From equation (2) one can see that this requirement is equivalent to conditions $\tau_s/\beta_2 \ll 1$ and $\kappa/\gamma \ll 1$, which are satisfied in our case ($\beta_2 \approx 100$ fs²).

The maximum average power from conventional Ti : Sa oscillators operating in the negative-dispersion regime (single-pulse in the cavity) cannot exceed 1 W because of multi-pulsing [27, 28]. But in the PDR (also single-pulse regime) this value can be increased up to several watts because of the long intracavity pulse, in agreement with the relation $P_{av} = P_{peak} T/T_{cav}$. In this relation, only P_{peak} is limited due to instability. On the basis of a technique reported in [29] one can achieve tens of μ J pulses by storing energy in an external cavity synchronized with a high-energy short-cavity oscillator.

4.6. Self-similar pulses and the PDR

A comparison of the chirped-pulse regime with the so-called regime of self-similar pulse evolution in a laser [2, 25] needs some comment. Our model based on the generalized Ginzburg–Landau equation (1) is truly distributed and does not need any variation of the parameters along a propagation axis in order to obtain parabolic-like spectra, as observed in the experiment. Therefore, the numerically obtained static solution of the distributed equation (1) can be treated as a quasi-soliton (not a breather or a self-similar pulse). Hence, the self-similarity phenomenon cannot be considered as a cause of the regime. The main causes providing the parabolic-like spectra are strong pulse chirp in the PDR and saturation of SAM (the quintic term in equation (1); without saturation only Π -shaped spectra are possible in the absence of high-order dispersion). In spite of the fact that the considered chirped-pulse regime is not related to the self-similar pulses, we suspect it could be useful in fibre oscillators, which have afforded good prospects of high-energy pulse generation [17, 30].

5. Conclusion

A detailed theoretical study of the PDR based on the distributed complex cubic–quintic Ginzburg–Landau model was conducted. Agreement with the experimental data resulted from careful estimation of the model parameters and correct choice of the gain saturation law.

It was demonstrated that there are three main spectral shapes (parabolic-like, Π - and M-like) varying with the dispersion. The parabolic-like spectrum can be formed only due to saturation of SAM; the M-shaped spectrum is caused by fourth-order dispersion.

It was found that dynamic gain saturation plays a decisive role in pulse stabilization. Together with SAM it defines the limits of spectrum broadening and pulse duration. As a result, stable high-energy operation in a sub-10 MHz oscillator is only possible with SBR.

The upper limit of the pulse energy was identified with the threshold peak power causing self-focusing inside an active medium. Since the pulse is heavily chirped and has a wide spectrum, it is compressible down to sub-30 fs. Generation of such short and high-energy pulses from low-repetition rate oscillators operating in the negative dispersion regime is an intractable problem.

It was found that the basic characteristics of the PDR, such as spectral shapes and widths, pulse chirp, duration and stability, are not related to the so-called self-similar pulse regime.

Further prospects for the PDR can be formulated in the following way. It is obvious that there is a natural upper limit for the cavity period: $T_{\text{cav}} < T_r$. In the vicinity of this limit, further energy increase can only be provided by higher average power (optimization of oscillator) with correspondingly longer pulses. In order to reach the widest spectrum in the vicinity of zero GDD, both SBR and fourth-order dispersion are required for pulse stabilization and spectral shaping. An analysis of the PDR for high-energy oscillators with SBR aimed at optimizing the SAM parameters will be presented elsewhere.

Acknowledgments

This work was supported by FWF (Austria) through grants Z63, F016 and P15382, by the Christian Doppler Society, and the European Community's Human Potential Programme under contract MRTN-CT-2003-50138 (XTRA). VLK acknowledges support from the Österreichische Forschungsgemeinschaft (grant MOEL080) and the Max-Planck-Gesellschaft.

References

- [1] Naumov S, Fernandez A, Graf R, Dombi P, Krausz F and Apolonski A 2005 *New J. Phys.* **7** 216
- [2] Ilday F Ö, Buckley J R, Clark W G and Wise F W 2004 *Phys. Rev. Lett.* **92** 213902
- [3] Ilday F Ö, Wise F W and Kaertner F X 2004 *Opt. Express* **12** 2731–8
- [4] Haus H A, Fujimoto J G and Ippen E P 1991 *J. Opt. Soc. Am.* B **8** 2068
- [5] Haus H A, Fujimoto J G and Ippen E P 1992 *IEEE J. Quantum Electron.* **28** 2086
- [6] Krausz F, Fermann M E, Brabec Th, Curley P F, Hofer M, Ober M H, Spielmann Ch, Wintner E and Schmidt A J 1992 *IEEE J. Quantum Electron.* **28** 2097
- [7] Herrmann J 1994 *J. Opt. Soc. Am.* B **11** 498
- [8] Kalashnikov V L, Kalosha V P, Poloyko I G and Mikhailov V P 1997 *J. Opt. Soc. Am.* B **14** 964
- [9] Christov I P and Stoev V D 1998 *J. Opt. Soc. Am.* B **15** 1960
- [10] Kalosha V P, Müller M, Herrmann J and Gatz S 1998 *J. Opt. Soc. Am.* B **15** 535
- [11] Haus H A 1975 *J. Appl. Phys.* **46** 3049
- [12] Akhmediev N N and Ankiewicz A 1997 *Solitons: Nonlinear Pulses and Beams* (London: Chapman and Hall)
- [13] Kalashnikov V L, Sorokin E and Sorokina I T 2001 *J. Opt. Soc. Am.* B **18** 1732
- [14] Chen Y, Kärtner F X, Morgner U, Cho S H, Haus H A, Ippen E P and Fujimoto J G 1999 *J. Opt. Soc. Am.* B **16** 1999
- [15] Proctor B, Westwig E and Wise F 1993 *Opt. Lett.* **18** 1654
- [16] Dudley J M, Bousson S M, Cameron D M J and Harvey J D 1999 *Appl. Opt.* **38** 3308
- [17] Peacock A C, Kruhlak R J, Harvey J D and Dudley J M 2002 *Opt. Commun.* **206** 171
- [18] Smolorz S and Wise F 1998 *Opt. Lett.* **23** 1381
- [19] Hocking L M and Stewartson K 1972 *Proc. R. Soc. Lond. A* **326** 289
- [20] Kalashnikov V L, Zhavoronkov N I, Poloyko I G and Mikhailov V P 1997 *J. Opt. Soc. Am.* B **14** 2705
- [21] Moores J D 1993 *Opt. Commun.* **96** 65
- [22] Herrmann J and Müller M 1996 *J. Opt. Soc. Am.* B **13** 1542

- [23] Soto-Crespo J M, Akhmediev N N and Afanasjev V V 1996 *J. Opt. Soc. Am. B* **13** 1439
- [24] Fernandez A, Fuji T, Poppe A, Fürbach A, Krausz F and Apolonski A 2004 *Opt. Lett.* **29** 1366
- [25] Wise F W, Ilday F Ö and Kärtner F X 2005 *Tech. Dig. Advanced Solid-State Photonics (Vienna)* p MF44
- [26] Kowalevich A M, Tucay Zare A, Kärtner F X, Fujimoto J G, Dewald S, Morgner U, Scheuer V and Angelow G. 2003 *Opt. Lett.* **28** 1597
- [27] Kalashnikov V L, Sorokin E and Sorokina I T 2003 *IEEE J. Quantum Electron.* **39** 323
- [28] Apolonski A 2000 private communication
- [29] Jones R J, Moll K D, Thorpe M J and Ye J 2005 *Phys. Rev. Lett.* **94** 193201
- [30] Buckley J R, Wise F W, Ilday F Ö and Sosnowski T 2005 *Opt. Lett.* **30** 1888